Analysis of neutral fragments from ultraviolet laser irradiation of a photolabile triazeno polymer

T. Lippert
Paul Scherrer Institut, 5232 Villigen PSI, Switzerland

S. C. Langford
Surface Dynamics Laboratory, Department of Physics and Materials Science Program, Washington State University, Pullman, Washington 99164-2814

A. Wokaun
Paul Scherrer Institut, 5232 Villigen PSI, Switzerland

Georgiou Savas
Institute of Electronic Structure and Laser, Foundation for Research and Technology–Hellas, 711 10 Heraklion, Crete, Germany

J. T. Dickinson[a)]
Surface Dynamics Laboratory, Department of Physics and Materials Science Program, Washington State University, Pullman, Washington 99164-2814

(Received 6 July 1999; accepted for publication 17 September 1999)

A photolabile triazeno polymer was irradiated with pulsed excimer laser light at 248 nm and 30 ns pulse width. The ablation fragments were analyzed using time-of-flight (TOF) mass spectrometry. At fluences below 1.3 J/cm^2, only neutral products were found. At these fluences, N_2 is by far the most intense neutral signal along with measurable phenyl radical (mass 76) production. The N_2 TOF shows a fast shoulder corresponding to kinetic energies of about 1.1 eV and a long slow tail persisting for hundreds of microseconds. The tail is attributed to delayed emission of reaction products from the polymer. The kinetic energy of the fast peak is attributed to direct ejection of products from surface sites undergoing exothermic decomposition. A weaker signal due to the phenyl radical is also observed. The observed fluence dependence of the two major products is highly nonlinear and is shown to fit an Arrhenius equation. We discuss the implications of these measurements regarding photochemical versus photothermal processes. © *1999 American Institute of Physics.* [S0021-8979(99)07924-4]

I. INTRODUCTION

Laser ablation of polymers has been studied extensively with various analytical techniques.[1] The ablation mechanisms, i.e., photothermal versus photochemical, are still often controversial. Srinivasan[2] has repeatedly emphasized the importance of looking at the product distribution in order to establish and/or test ablation mechanisms. Mass spectrometric studies have been performed on various polymers under various conditions, e.g., as a function of irradiation wavelength and laser fluence.[3] Analysis of the ejected material has revealed ionic and neutral species with masses ranging from small degradation fragments,[4,5] to the monomer (from unzipping reactions),[6,7] to carbon clusters,[8] and finally to polymer fragments with molecular weights of up to 2500.[9,10] Time-of-flight (TOF) distributions (in reality, these are ''time-of-arrival'' curves) of neutral fragments have been analyzed to determine the energy distributions of the fragments. For several polymers such as polystyrene, Teflon, and polymethyl methacrylate (PMMA), Maxwell–Boltzmann distributions were obtained, yielding temperatures compatible with photothermal decomposition.[11–13] In the case of polystyrene irradiated at 193 nm, an adiabatic expansion model inferred temperatures of ~2350 K.[14] When absorbing chromophores were purposefully added to PMMA, a combined photochemical/photothermal mechanism was evident.[15]

In general, most TOF-mass spectrometer (MS) studies have given strong indications for photothermal ablation mechanisms. To test whether a photochemical mechanism could be identified with TOF-MS, we chose a polymer considered photolabile, which also has excellent properties as a resist for high-resolution microlithography.[16] Here, we show that the principle products (chiefly N_2) from this triazeno polymer have components that are much more energetic than expected for thermal products. Further, the fluence dependence of the emissions is a strongly nonlinear function of fluence, again suggestive of a nonthermal decomposition mechanism. Nevertheless, an Arrhenius description [used previously for the UV laser induced products from polytetrafluoroethylene (PTFE)[6]], assuming an activation energy equal to the thermal decomposition energy of the polymer, yields a good description of the emission intensities. We tentatively conclude that the photothermal aspects of this process dominate.

[a)]Electronic mail: jtd@wsu.edu

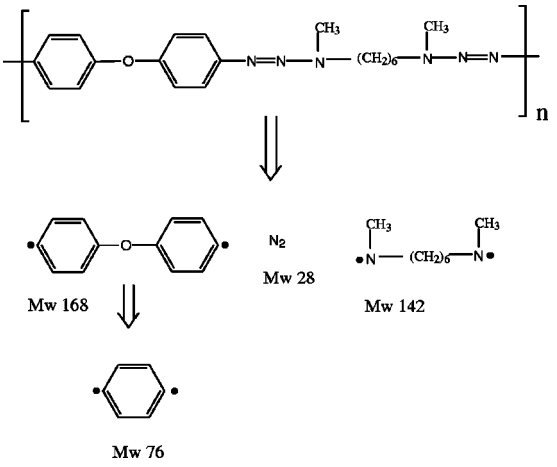

FIG. 1. Chemical structure and a possible decomposition scheme for the triazenopolymer.

II. EXPERIMENT AND CURVE FITTING

The chemical structure of the polymer is diagramed in Fig. 1. Its average molecular weight is about 71 000 g/mole, corresponding to about 190 monomer units (n in Fig. 1). Synthesis of the polymer is described elsewhere.[17] Thin films (several hundred μm thick) of the polymer were prepared by solvent casting onto a polypropylene substrate. It should be noted that the decomposition of the monomer is exothermic with a decomposition enthalpy of -624 J/g.[18] The absorption coefficient at 248 nm is $\sim 66\,000$ cm^{-1}, which is quite high; nevertheless, it is not at the maximum (typically at wavelengths in the 310–350 nm region).

The experimental arrangement has been described previously.[19] The polymer films were irradiated at 248 nm at a pulse repetition rate of 1 Hz to avoid accumulative heating. Emissions were detected with a quadrupole mass spectrometer (UTI 100C) mounted with the ionizer 30 cm from the sample. Time-resolved quadrupole mass spectroscopy was used to simultaneously measure both the charge to mass ratio (m/z) and the time-of-flight distributions of the emitted species. Curve fitting techniques were employed to test various models of the emission process.

Nitrogen molecules emitted from the polymer showed both highly energetic components (short TOF) and very slow components consistent with emission long after the laser pulse. The overlap between the fast and slow components, and the fact that a large majority of the total counts reside in the slow component, make it particularly important to describe the leading edge of the slow component accurately in order to characterize the fast component. To carry this out, a number of models were tested by curve fitting the acquired TOF curves.

The model employed below assumed that the emission intensity of the slow component was controlled by a thermally activated process (which we assume is decomposition limited but could be diffusion limited) which continued after the laser pulse. That is, the emission rate, $S(t')$ is given by

$$S(t') \sim S_0 \exp(-E_a/kT), \tag{1}$$

where Ea is an activation energy, k is Boltzmann's constant, and T is the surface temperature. The laser will heat the surface to some temperature $T_{\mathrm{RT}}+\Delta T$ (where T_{RT}=room temperature) and the surface subsequently cools. The emission rate is a strong function of how the sample cools, which in turn depends on the initial temperature distribution. We assume that laser heating is initially confined to a surface layer of depth a. This initial temperature distribution is consistent with the highly absorbing nature of the polymer. At the fluences employed in this work, the absorbing centers should be ''saturated'' to a significant depth. If the saturated material lacks the ability to absorb additional photons (which may require the absorption of more than one photon), the depth of the heated region should be a strong function of laser fluence, while the temperature of the heated material remains roughly constant (determined by the chromophore concentration and the number of photons required to saturate the chromophores). Under these conditions, the surface temperature after the laser pulse varies as

$$T = T_{\mathrm{RT}} + \Delta T \,\mathrm{erf}\left(\frac{a}{2\sqrt{\kappa t}}\right) = T_{\mathrm{RT}} + \Delta T \,\mathrm{erf}\left(\frac{\alpha}{\sqrt{t}}\right), \tag{2}$$

where κ is the thermal diffusivity, t is the time since the laser pulse, and $\alpha = 1/2\sqrt{\kappa}$, the actual fit parameter employed in modeling. Although the physical model (and the number of parameters) may seem to be unnecessarily complex, the resulting equations displayed good behavior when fits to the slow tail were extrapolated back into the fast/slow overlap region. This is not the case with several simpler models, including those based on linear, Beer's law absorption.

To predict the actual detected signal, $I(t)$, at the detector position relative to the sample (x,y,z), the emission rate was convoluted with the Maxwell–Boltzmann velocity distribution, $\mathrm{MB}(t-t')$,

$$I(t) = \int_0^t S(t')\,\mathrm{MB}(t-t')\,dt', \tag{3}$$

where $\mathrm{MB}(t-t')$ is given by

$$\mathrm{MB}(t-t') = \frac{x}{2\pi(t-t')^4}\left(\frac{m}{kT}\right)^2 \times \exp\left(\frac{-m(x^2+y^2+z^2)}{2kT(t-t')^2}\right). \tag{4}$$

S_0, E_a, ΔT, and α were determined by least-squares fitting techniques.[20]

Extrapolating this model to short times produced a physically plausible leading edge to the slow emission component, allowing for a reasonable description of the fast component. The fast component was described by assuming that the emitted N_2 had a Gaussian energy distribution with amplitude A, most probable energy E_0 and standard deviation σ, where all particles are emitted during the laser pulse (a delta function in time). This distribution is readily transformed to yield a particle density at the ionizer vs. time.

Experimentally, the analysis of the fast component is complicated by the delay between particle ionization [with

the rate given by Eq. (4)] and particle detection at the exit aperture of the quadrupole mass filter. Ionized particles entering the mass filter gain a kinetic energy of 15 eV, which is much greater than the kinetic energies of typical particles with effective temperatures below a few thousand K. Thus, for thermal distributions, the travel time through the mass filter is essentially constant and can be simply subtracted from the arrival time at the detector. However, particle velocities (before ionization) in the fast component are much higher and significantly affect the travel time through the quadrupole mass filter. The travel time through the mass filter for these particles was determined by solving the appropriate fourth-order equation by iteration for each data point.

III. RESULTS AND DISCUSSION

Photodecomposition of the polymer is expected to yield significant amounts of volatile N_2 (28 amu) phenyl radicals (76 amu) via the proposed reaction pathways shown in Fig. 1. Other low molecular weight species are also expected (e.g., various CH fragments), but in most cases it is not clear whether these other fragments were created during ablation or are cracking fractions created by electron impact ionization. Therefore, we focus our attention on N_2 and the phenyl radical. No intact repetition units were found among the ablation fragments, presumably due to the photolabile character of the triazeno units ($R-N^1=N^2-N^3<$) of which two are found in each repetition unit. The photochemistry of the triazeno group in monomeric compounds has been previously studied in detail. The first step of UV photodecomposition involves homolytic bond breakage between the N^2 and N^3 ($R-N^1=N^2\cdot\cdot N^3<$) nitrogen atoms, creating two radicals.[21,22] The diazo radical is quite unstable and would be expected to decompose by elimination of N_2, creating $R\cdot$ species which have been detected by electron spin resonance (ESR).[21,22]

The neutral fragments observed during UV laser ablation of the polymer are in fact compatible with this decomposition mechanism. The two fragments with the highest intensities are N_2 ($m/z=28$ amu/e) and the phenyl fragment ($m/z=76$ amu/e). Two molecules of each species can be liberated by the decomposition of each repetition unit. N_2 is chemically inert and relatively stable during electron impact ionization. Similarly, the phenyl fragment, like most aromatic compounds, shows a very stable parent molecular ion. In contrast, aliphatic compounds like the aliphatic amino fragment ($m/z=142$) undergo extensive fragmentation in the ionizer. Phenyl fragments can also be formed by fragmentation of intact diphenyl ether fragments ($m/z=168$) during electron impact ionization or during laser induced decomposition. The diphenylether fragment ($M_w=168$) absorbs strongly at 248 nm, which would promote dissociation into phenyl fragments.

By far, the most intense neutral signal is due to N_2. Figure 2 compares the time-of-flight curves for N_2 at three fluences. Only the first 500 μs of data are shown. Over this time interval, the great majority of the detected signal can be attributed to N_2 emitted directly from the sample, as opposed to molecules bouncing off the chamber walls. (This was verified by performing identical TOF measurements after blocking the direct path between the sample and the ionizer.)

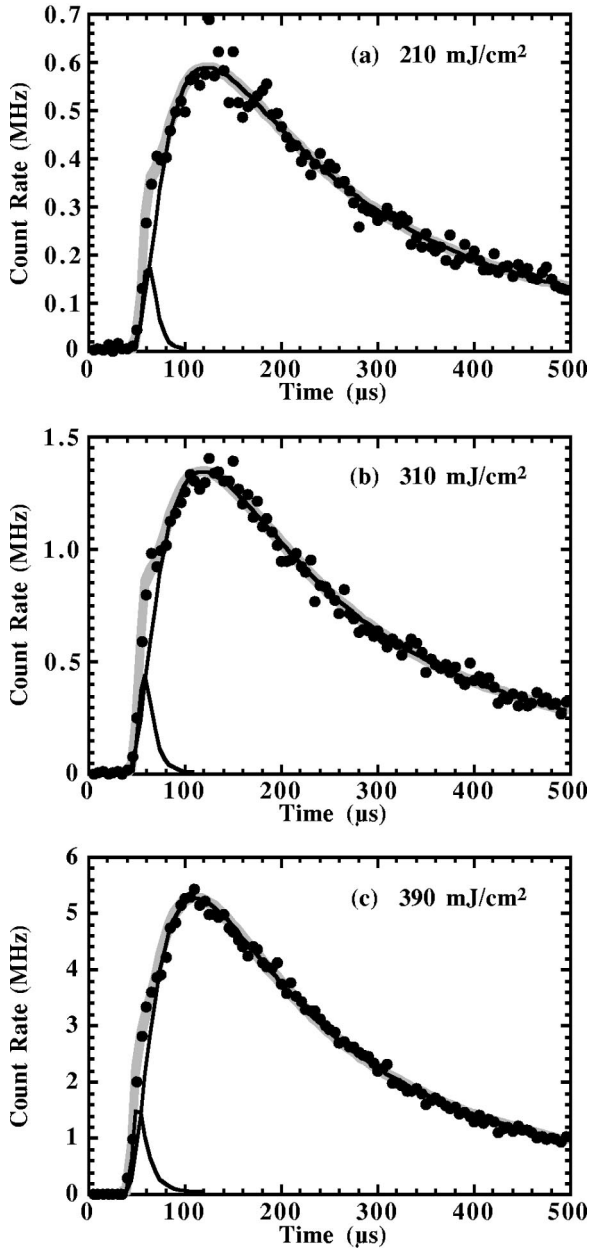

FIG. 2. Time-of-flight signals for N_2 at three laser fluences. A curve fit to the data using a Gaussian energy distribution for the shoulder and Eq. (3) for the slow peak is shown in the light, broad line; the individual fast and slow components are shown as dark lines.

All three TOF curves in Fig. 2 show a distinctive shoulder on the fast leading edge, followed by a broad peak and long tail. The particles in the shoulder are moving extremely fast; the position of the shoulder corresponds to a kinetic energy above 0.7 eV. The Gaussian energy distributions used to model these fast peaks are also shown in Fig. 2. At the lower fluences, where the effect of gas phase collisions on the energy distributions can be neglected, the center (mean) energy of the Gaussian distributions correspond to 1.1 ± 0.1 eV. These energies are well above those expected for typical thermal processes, and are presumably due to the concerted motion of decomposition fragments. That is, the reaction

fragments depart from the parent molecule without colliding with other particles; these particles are not ''thermalized'' and display kinetic energies comparable to the loss of potential energy in the exothermic decomposition reaction. Similar TOF curves have been observed for reaction fragments following the IR induced, exothermic decomposition of molecular cyclotrimethylene-trinitramine (RDX), an energetic compound used in explosives and rocket propellants.[23] UV laser irradiation (248 nm) of solid RDX single crystals yielded a number of product species exhibiting both a ''hot and cold'' component.[24]

The broad peak and tail in the N_2 TOF distribution are much broader than Maxwell–Boltzmann distributions with similar peak TOFs. Nevertheless, the peak TOF does shift to shorter times with increasing fluence. This shift is often associated with thermal emission, where higher fluences produce higher surface temperatures and thus faster particles. In such cases, long emission tails are often associated with emission *after* the laser pulse.[25,26] For instance, either a thermal decomposition rate decreasing in time due to cooling or the diffusion of volatile species (produced in the bulk of the polymer) to the surface could explain a slowly decaying component of emission that persists long after the laser pulse. Estimates of the total yield of N_2 per laser pulse exceed 10^{15} molecules/cm^2 as the fluence is increased to 310 mJ/cm^2. At this particle density, collisions among the emitted N_2 molecules are expected to modify the original (as emitted) velocity distribution.[27]

Weaker emissions at 76 amu (the phenyl radical) are also observed. Typical TOF distributions are shown in Fig. 3. Note that higher fluences are employed in these measurements to provide measurable signals for analysis. Again, the leading edge of the TOF distribution is fast. The maximum particle velocities at this mass are only slightly less than the maximum N_2 particle velocities at the same fluence. The higher mass of the phenyl radical ensures that the energies of the fastest phenyl radicals are much higher than the energies of the fastest N_2 molecules. We attribute the high velocities of the fastest phenyl radicals to collisions with fast N_2 molecules leading to entrainment of the heavier molecules. In the limit of large numbers of collisions, the fast N_2 and fast phenyl radicals will move with very nearly the same velocities, as observed. (This process is exploited to accelerate massive molecules to high kinetic energies, by entraining them in a supersonic molecular beam formed by free adiabatic expansion of a light gas such as helium.) As noted above, the N_2 densities at the lowest fluence displayed in Fig. 3 (310 mJ/cm^2) are adequate to account for such a collisional acceleration of the phenyl radicals. Like the N_2, the phenyl radicals also display a long tail, consistent with slowly decaying emission intensities long after the laser pulse. The phenyl intensities were typically less than 1% of the N_2 intensities at the same fluence.

The intensities of both N_2 and phenyl radicals depend strongly on fluence. Their fluence dependence is displayed as log-log plots in Fig. 4. As discussed above, N_2 is much more intense than the phenyl radical (by almost two orders of magnitude) and is first detected at considerably lower fluences. Much of this intensity difference can be attributed to

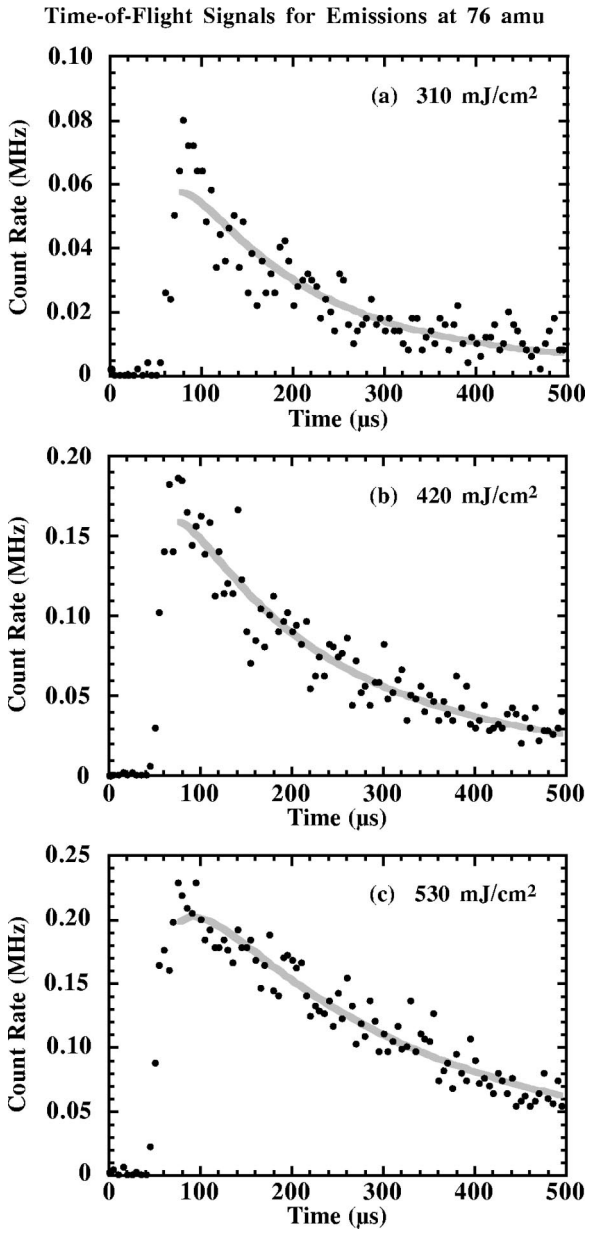

FIG. 3. Time-of-flight signals for the phenyl radical at three laser fluences. A curve fit to the data using Eq. (3) is shown in the light, broad line.

differences in the survival and ionization probabilities of the two species. Thus, it is not clear how much of the apparent difference in emission threshold for N_2 and phenyl radicals in Fig. 4 is due to different emission intensities versus different detection probabilities. Since two N_2 molecules must be emitted to release one phenyl radical, some difference in fluence dependence is expected. For both species, the intensity rises above the background in approximately power law fashion. Finally, at still higher fluences, the intensity rolls over, growing more slowly with increasing fluence. The slopes of the ''power-law'' portions of the two plots are 8 for N_2 and $\sim$12 the phenyl radical, respectively. Although we could suggest that this corresponds to an 8 and 12 photon process (either multiphoton or multiple photon), this seems totally unacceptable and unreasonable. Furthermore, it is inconsistent with a simple photodecomposition mechanism

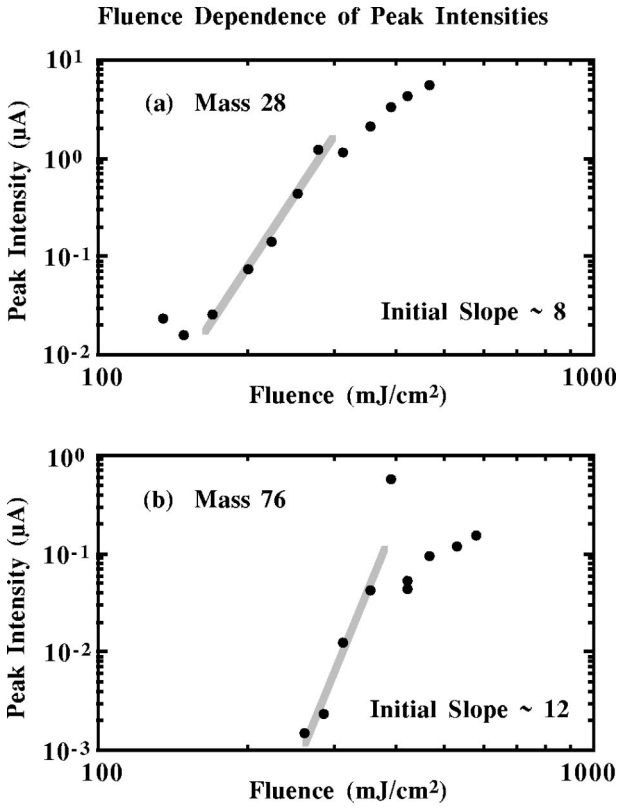

FIG. 4. Log-log plots of the signal intensities for the two principal fragments (a) N_2 (28 amu) and (b) the phenyl radical (76 amu), as a function of laser fluence.

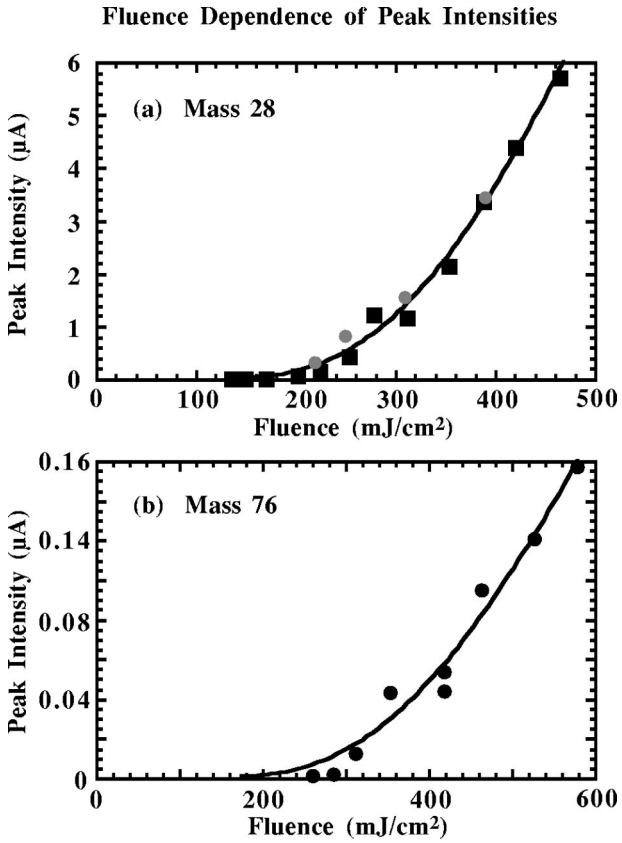

FIG. 5. Linear plots of the signal intensities for the two principal fragments (a) N_2 (28 amu) and (b) the phenyl radical (76 amu), as a function of laser fluence. The dark line shows a least-squares fit of the data to a thermal model for emission, assuming an activation energy of 2.1 eV (the thermal activation energy for polymer decomposition). The gray dots in (a) indicate the area of the N_2 fast peak determined from curve fits to the TOF data.

where we would expect the number of product molecules (broken bonds) to be first order in the laser fluence.

An alternative mechanism to explore in terms of this fluence dependence is a photothermal mechanism which we propose would fit an Arrhenius equation.[6] For a single photon photothermal process, where all absorbed light goes into heat, and neglecting thermal diffusion, the temperature rise can be expressed in terms of the absorption coefficient, α:

$$\Delta T = \frac{F_0(1-R)\alpha}{\rho C_v}, \tag{5}$$

where F_0 is the laser fluence at the sample surface, R is the surface reflectivity at the laser wavelength, ρ is the sample density, and C_v=heat capacity of the sample. Thermal diffusion can be neglected if the conduction during the laser pulse is less than the laser spot size or the thickness of the heated layer. This is ensured if the characteristic thermal diffusion length, $(2\kappa\tau)^{1/2}$ (where κ is the thermal diffusivity of the polymer and τ is the laser pulse width—30 ns), is much less than the radius of the laser spot (500 μm) and the thickness of the heated layer ($\sim\alpha^{-1}\sim$170 nm). Assuming that the thermal properties of this polymer are similar to polycarbonate or polyethylene, the characteristic diffusion length is on the order of 60 nm during the laser pulse. This is indeed much smaller than the laser spot size and significantly smaller than the expected thickness of the heated layer.

Using this temperature, an Arrhenius-like description of the emission intensity yields

$$I(t) = A \exp\left[\frac{-E_a}{k(T_{\mathrm{RT}}+\Delta T)}\right], \tag{6}$$

where E_a is the activation energy. In principle, one can determine E_a by fitting Eq. (6) to the data, but a more stringent test of the thermal decomposition hypothesis is obtained if we fix E_a to the known activation energy for thermal decomposition for this material ($E_a\sim$2.1 eV). Equation (6) was then fit to the intensity versus fluence data [with the omission of an outlier data point in Fig. 4(b)] and the results are shown in Fig. 5. Although one might argue that the data systematically depart from the model at the lower fluences, the fluence range adequately treated by Eq. (6) is significantly greater than the ''power law'' region of Fig. 4. Furthermore, we can plot the intensities of the mass 28 fast component at the lower laser fluences. These data are shown by the gray dots in Fig. 5(a) and are seen to fall directly on the Arrhenius equation fit. Our conclusion is that a thermal-activation model describes the intensity versus fluence data quite adequately.

The predicted temperature rise from Eq. (6) provides a check on the physical reasonableness of a thermal activation description. At a fluence of 400 mJ/cm^2, both curve fits in Fig. 5 indicate a temperature change of about 6000 K. This is on the high end of what one might consider to be physical temperature values. However, it is consistent with tempera-

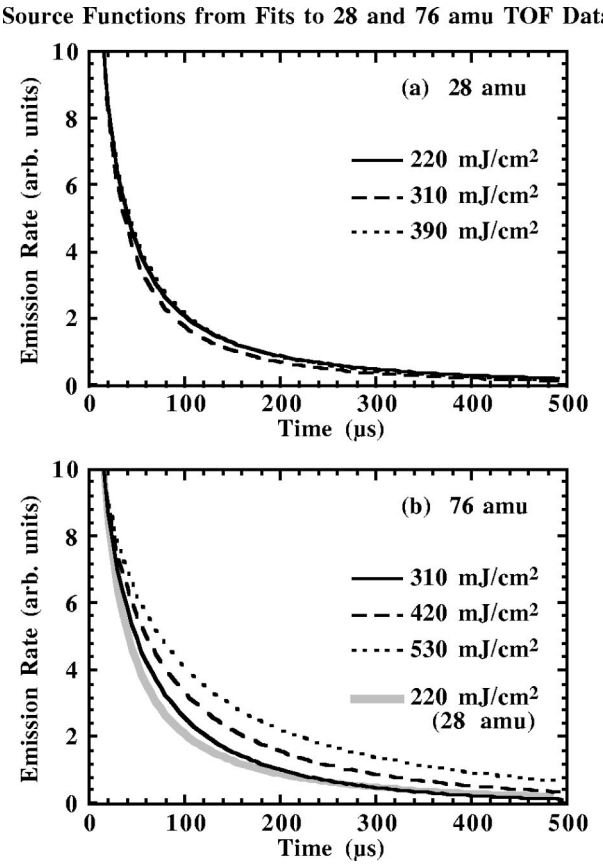

FIG. 6. Plots of the source functions determined from fitting Eq. (3) to the TOF data of (a) Fig. 2 (N_2) and (b) Fig. 3 (phenyl radical), all normalized to the same initial intensity. The N_2 source function at 220 mJ/cm^2 is also plotted as the light line in (b) to facilitate comparison of the N_2 and phenyl radical source functions.

tures predicted by curve fits to individual TOF curves at this fluence using Eq. (3). We also note that decomposition measurements on second to minute time scales (as in differential scanning calorimetry) yield much lower decomposition temperatures (500–550 K). Due to the short time scales for heating during laser ablation, much higher temperatures are required for observable decomposition. Improved thermal models would better predict the duration of heating, which depends on the depth of the heated layer [as in Eq. (2)].

The slow decay of the N_2 and phenyl emissions after the laser pulse requires emission after the laser pulse. (Although collisions can slow particles as well as speed them up, the net effect in TOF measurements is to shift the peak TOF to shorter times.[2] Collisions cannot explain the long tails.) The duration of this emission can be estimated from the source function used to describe the slow tails [Eq. (1)]. The fast molecules were excluded from the analysis by considering only those particles arriving at least 80 μs after the laser pulse. The source functions corresponding to the data of Figs. 2 and 3 are shown in Fig. 6, all normalized to unit intensity at time $t=0$. The source functions for N_2 are all very similar to each other and to the low-fluence source functions for the phenyl radical. [The low-fluence N_2 source function is displayed for comparison with the phenyl source functions as the light, broad line in Fig. 6(b).] At higher fluences, the phenyl radical source functions extend to slightly longer times. At low fluences, the emission of N_2 and phenyl radicals are very likely controlled by the same process. This tail is in fact entirely consistent with the proposed thermal decomposition rate [Eq. (6)] decaying due to cooling of the surface given by Eq. (2).

IV. CONCLUSION

In summary, mass-selected TOF measurements during the UV laser (248 nm) induced decomposition of a photolabile polymer show fast neutral particles which are most likely due to particles emitted directly from the surface by a concerted, exothermic chemical reaction. At this point, time-of-flight measurements cannot distinguish whether this reaction is initiated directly by photon absorption (photochemical dissociation) or exothermic decomposition induced by thermal excitation. Importantly, the fast mass 28 (N_2) component, the total mass 28 (N_2) emission, *and* the total mass 76 (phenyl radical) emission all follow an Arrhenius relation where the temperature is predicted from the total laser energy deposited. We therefore propose that photothermal processes are dominating the rates of formation of these products. The fast component of N_2 emission may then be attributed to a thermally induced exothermic decomposition where the products come off prior to equilibriating with the surface. The cooling of the surface [Eq. (2)] explains the slow tail in the emission that follows the laser pulse (by as much as a hundred microseconds), e.g., seen in Fig. 6.

We are currently exploring the use of low temperatures (i.e., 77 K) and using low fluences to attempt to suppress the thermal processes. Furthermore, in the case of triazeno polymers, we also expect stronger signals due to irradiation at 308 nm, near a maximum in the photodissociation cross section. These experiments may also provide us more information on the significance of gas-dynamic processes among the emitted fragments, where a substantial population of phenyl radicals appear to have been accelerated by entrainment, perhaps by reducing the density of the emitted N_2 to where we might be able to see the direct phenyl radical time of flight. It is possible, as proposed in an earlier laser-polymer study,[15] that *both* photochemical and photothermal mechanisms are occurring.

ACKNOWLEDGMENTS

One of the authors (T.L.) wishes to express his gratitude to Los Alamos National Laboratory for a research fellowship during part of this work. This investigation was supported in part by the Department of Energy, Basic Energy Sciences, under Contract No. DE-FG03-98ER14864 and a NATO Collaborative Science and Technology Grant.

[1] R. Srinivasan and B. Braren, Chem. Rev. **89**, 1303 (1989).
[2] R. Srinivasan, Appl. Phys. A: Solids Surf. **56**, 417 (1993).
[3] F. Kokai, Y. Koga, Y. Kakudate, M. Kawaguchi, S. Fujiwara, M. Kubota, and M. Fukuda, Appl. Phys. A: Solids Surf. **59**, 299 (1994).
[4] R. C. Estler and N. S. Nogar, Appl. Phys. Lett. **49**, 1175 (1986).
[5] D. J. Krajnovich, J. Phys. Chem. A **101**, 2033 (1997).
[6] J. T. Dickinson, J.-J. Shin, W. Jiang, and M. G. Norton, J. Appl. Phys. **74**, 4729 (1993).
[7] G. B. Blanchet and J. C. R. Fincher, Appl. Phys. Lett. **68**, 929 (1996).

[8] S. G. Hansen, J. Appl. Phys. **66**, 1411 (1989).
[9] R. Srinivasan, B. Braren, D. E. Seeger, and R. W. Dreyfus, Macromolecules **19**, 916 (1986).
[10] R. Larciprete and M. Stuke, Appl. Phys. B: Photophys. Laser Chem. **42**, 181 (1987).
[11] M. Tsunekawa, S. Nishio, and H. Sato, J. Appl. Phys. **76**, 5598 (1994).
[12] M. Tsunekawa, S. Nishio, and H. Sato, Jpn. J. Appl. Phys., Part 1 **34**, 218 (1995).
[13] B. Danielzik, N. Fabricius, M. Röwekamp, and D. v. d. Linde, Appl. Phys. Lett. **48**, 212 (1986).
[14] D. Feldmann, J. Kutzner, J. Laukemper, S. MacRobert, and K. H. Welge, Appl. Phys. B **44**, 81 (1987).
[15] T. Lippert, J. Appl. Phys. **85**, 1838 (1999).
[16] T. Lippert, J. Stebani, J. Ihlemann, O. Nuyken, and A. Wokaun, J. Phys. Chem. **97**, 12296 (1993).
[17] J. Stebani, O. Nuyken, T. Lippert, and A. Wokaun, Makromol. Chem., Rapid Commun. **206**, 2943 (1993).
[18] Y. Ben-Eliahu, Y. Haas, and S. Welner, J. Phys. Chem. **99**, 6010 (1995).
[19] J. J. Shin, D. R. Ermer, S. C. Langford, and J. T. Dickinson, Appl. Phys. A: Mater. Sci. Process. **64**, 7 (1997).
[20] W. H. Press, B. P. Flannery, S. A. Teukolsky, and W. T. Vetterling, *Numerical Recipes in Pascal: The Art of Scientific Computing* (Cambridge University, Cambridge, 1989).
[21] T. Lippert, J. Stebani, A. Stasko, O. Nuyken, and A. Wokaun, J. Photochem. Photobiol. A **78**, 139 (1994).
[22] A. Stasko, V. Adamcik, T. Lippert, A. Wokaun, J. Dauth, and O. Nuyken, Makromol. Chem. **194**, 3385 (1993).
[23] X. Zhao, E. J. Hintsa, and Y. T. Lee, J. Chem. Phys. **88**, 801 (1988).
[24] J. T. Dickinson, L. C. Jensen, D. L. Doering, and R. Yee, J. Appl. Phys. **67**, 3641 (1990).
[25] R. L. Webb, S. C. Langford, and J. T. Dickinson, Nucl. Instrum. Methods Phys. Res. B **103**, 297–308 (1995).
[26] J. T. Dickinson, J.-J. Shin, and S. C. Langford, Appl. Surf. Sci. **96–98**, 326 (1996).
[27] R. Kelly and R. W. Dreyfus, Nucl. Instrum. Methods Phys. Res. B **32**, 341 (1988).